Title

Common Photo-oxidative Decarboxylation Mechanism in Iron Hydroxy Carboxylate Complexes

Journal

The Journal of Physical Chemistry A, 127(30)

ISSN

1089-5639

Authors

Joe-Wong, Claresta
Schaller, Richard D
Gilbert, Benjamin

Publication Date

2023-08-03

DOI

10.1021/acs.jpca.3c02656

Common Photo-Oxidative Decarboxylation Mechanism in Iron Hydroxy Carboxylate Complexes

Claresta Joe-Wong[1], Richard D. Schaller[2], and Benjamin Gilbert[1,]*

[1]Energy Geoscience Division, Lawrence Berkeley National Laboratory, 1 Cyclotron Road, Berkeley, CA 94720

[2]Center for Nanoscale Materials, Argonne National Laboratory, 9700 South Cass Avenue, Building 440, Argonne, IL 60439, USA

* Corresponding author: bgilbert@lbl.gov

ABSTRACT

Photochemical oxidation of dissolved organic matter is a crucial component of carbon cycling in surface waters. Photo-oxidation of iron(III)-carboxylate complexes is of particular interest because complexation with iron(III) can sensitize this functional group to photo-decarboxylation. The photo-oxidation mechanism of ferrioxalate has been extensively characterized, but it is unclear whether the mechanism or timing is similar for other, more complex carboxylates. In this study, we use time-resolved infrared spectroscopy to demonstrate that Fe(III)-citrate, an aliphatic carboxylate, and Fe(III)-salicylate, an aromatic carboxylate, follow the same photo-oxidation kinetics as ferrioxalate. Hence the data suggest a common mechanism for decarboxylation for iron hydroxy carbonates. Differences in the CO_2 yield within 50 ps are qualitatively similar to the long-time-scale quantum yield for Fe(II) production.

INTRODUCTION

Photochemical oxidation of dissolved organic matter (DOM) in surface waters and atmospheric aerosols is a major pathway for the conversion of organic molecules or moieties to carbon dioxide (CO_2). [1,2] Photochemical fluxes of CO_2 can be a significant portion of total emissions from some environments, [3,4] but light-driven mineralization pathways remain poorly understood. [5] The sensitivity of DOM to photo-oxidation depends on many environmental conditions, such as pH and the presence of metal ions. [6-9] In particular, iron (Fe) forms complexes with DOM carboxylate moieties, [10,11] which can enhance DOM photoreactivity. [7,12] Many Fe(III)-organic compounds strongly absorb light in the UV-visible range, and photoexcitation can lead

ligand-to-metal charge transfer that reduces Fe(III) to Fe(II) and oxidizes the organic ligand. [1,13] Photolysis of Fe-carboxylate complexes can lead to decarboxylation, in which the COOH group is released as CO_2. [14] Decarboxylation reactions have been estimated to account for the majority of CO_2 emissions from photo-oxidized DOM, [15] potentially making Fe a critical component in DOM photo-oxidation in natural systems.

Photo-oxidation of ferrioxalate, $[Fe(III)(C_2O_4)_3]^{3-}$, has been well studied[12–15] because it is used as a chemical actinometer to quantify the flux of light. Furthermore, oxalic acid is the smallest aliphatic dicarboxylic acid that is commonly found in natural systems. [16] An unambiguous description of the initial mechanism of ferrioxalate photolysis has recently been obtained by us[17] and another group[18] using time-resolved infrared (IR) spectroscopy complemented by molecular simulation. In contrast to time-resolved optical[13,19] or X-ray methods [20] previously used to study ferrioxalate photolysis, time-resolved IR spectroscopy reveals shifts, losses or gains in vibrational modes associated with molecular species that participate in a light-initiated reaction. In brief, these studies discovered that intramolecular electron transfer from oxalate to Fe(III) takes place on a sub-picosecond timescale and is followed by lysis of the unstable oxalate radical anion to form a vibrationally excited CO_2 molecule and a CO_2^- radical anion. [17,18] The oxalate radical anion is not stable enough to be considered a relevant transient species, ending a longstanding debate. Due to the lack of other relevant studies, however, it is unknown whether the ferrioxalate photolysis mechanism is a broadly applicable model for other Fe(III)-carboxylate complexes.

In this study, we used time-resolved IR spectroscopy to examine the photo-decarboxylation mechanisms of Fe(III)-citrate and Fe(III)-salicylate. Citrate is an aliphatic α-hydroxy carboxylate that, like oxalate, is commonly found in natural environments (**Figure 1**), [16] but its higher molecular weight may make it a better proxy for aliphatic DOM molecules. Salicylate is also common in natural systems[16] but unlike oxalate and citrate is a β-hydroxy carboxylate with an aromatic ring (**Figure 1**). The differences in structure between these three molecules cause significant differences in quantum yield, as measured by the production of Fe(II) (oxalate > citrate $\gg$ salicylate).[10,21] However, it remains unclear whether the structural differences affect the reaction mechanism or kinetics of photo-decarboxylation. Here, we show that photo-decarboxylation of Fe(III)-citrate and Fe(III)-salicylate follow the same pathway and timing as ferrioxalate, which suggests that this mechanism may be broadly applicable to environmentally relevant carboxylates bound to Fe(III).

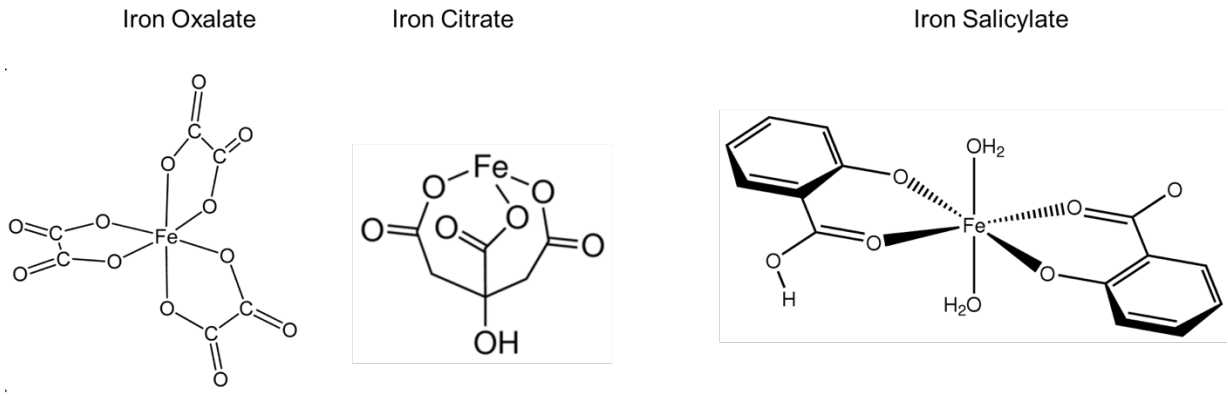

Figure 1 Examples of the molecular structures of ferrioxalate, Fe-citrate, and Fe-salicylate expected to form in solution under the analysis conditions. Iron citrate, in particular, may adopt multiple complex stoichiometries and structures in aqueous solutions [21].

MATERIALS AND METHODS

Sample synthesis and characterization

Stock solutions consisted of 0.1 M iron(III) chloride (Sigma-Aldrich, ACS reagent, 98.0-102% Fe(III) by redox titration), oxalic acid dihydrate (Sigma-Aldrich, ACS reagent, >99% purity), sodium citrate monobasic (Sigma-Aldrich, purum, anhydrous, ≥99.0% by base titration), and sodium salicylate (Sigma-Aldrich, Reagent Plus, >99.5% purity) in either H_2O (MilliQ purification system) or D_2O (Cambridge Isotope Laboratory or Aldrich). Stock solutions were mixed in the appropriate proportions to generation sample solutions of 100 mM ferrioxalate, iron(III) citrate, or iron(III) salicylate in H_2O or D_2O. Reference Fourier transform infrared (FTIR) spectrum of a 20-mM Fe-citrate solution was acquired using a Nicolet instrument with a diamond attenuated total reflectance (ATR) crystal.

Time-resolved infrared spectroscopy

Data acquisition.

Time-resolved (TR) infrared (IR) pump-probe spectroscopy was performed at the Center for Nanoscale Materials at Argonne National Laboratory. An amplified femtosecond Ti/sapphire laser system at 2 kHz generated pump pulses at 800nm that were frequency tripled to produce 266 nm and an optical parametric generator with difference frequency mixing of signal and idler produced mid-IR probe pulses. The interval between pump and probe pulses was controlled between -1.5 ps and 3 ns by a mechanical delay line. The time resolution was 100 fs. [22] TR-IR spectroscopy was performed on solutions of all three compounds in H_2O with the probe wavelength centered at 6900

nm (1449.3 cm^{-1}) to study CO_2 generation. TR-IR spectroscopy was performed on a solution of citrate in D_2O with the probe wavelength centered at 5996 nm (1667.8 cm^{-1}) to study carboxyl group changes.

Data analysis

Replicate transient absorption scans were averaged using Surface Explorer software and further processed using code written in IgorPro software. The pre-pump pulse background spectrum was subtracted from spectra at all time points, and spectra were extracted as unaveraged line scans. Time-dependent data were averaged over ~20 cm^{-1} of spectral bandwidth. These averaged traces still contained significant non-random noise apparently attributable to changes in detector gain between pixel elements. These effects were substantially corrected for by subtracting a control time-dependent trace at a wavenumber where no spectral changes were detected from the trace at a wavelength of a time-varying molecular vibration. For example, the CO_2 signal was revealed by subtracting a trace centered at 2302 cm^{-1} from the trace centered at 2339 cm^{-1}, the location of the CO_2 asymmetric stretch.

The time-dependent data for the 3 compounds were qualitatively compared by applying a multiplicative factor the minimized the sum of the squares of the intensity difference at each point. The time-dependent data were quantitative analyzed by fitting two models. The first assumes that CO_2 generation rate is determined by the decay of a photoexcited iron complex and is given by a first-order chemical kinetics expression (**Eqn. 1**)

Eqn. 1. $$I_{CO_2}=I^0_{CO_2}+C^{max}_{CO_2}(1-e^{tk_{1st}})$$

where $C^{max}_{CO_2}$ is the maximum signal observed at 2339 cm^{-1} after ~50 ps, k_{1st} is the rate constant and I^0 and C are constants. The second model assumes that photolysis occurs concurrently with photoexcitation and the increase of the CO_2 signal at 2339 cm^{-1} is determined by relaxation from two vibrationally excited states, and is given by a bi-exponential decay (**Eqn. 2**).

Eqn. 2. $$I_{CO_2}=I^0_{t0}+I^0_{t1}(1-e^{tk_{10}})+I^0_{t2}(1-e^{tk_{20}})$$

where k_{10} and k_{20} are the vibrational decay rate constants for the 1→0 and2→0 transitions, respectively, and the I^0's are constants. In agreement with prior work on ferrioxalate, the bi-exponential decay model gave improved fits to the data.

RESULTS AND DISCUSSION

Photoexcitation of Fe citrate in H_2O promptly generated CO_2, as shown by the appearance of a new vibrational signal with a maximum at 2339 cm^{-1} (**Figure 2A**). A signal with identical lineshape was observed for the photolysis of ferrioxalate in prior work[17,18] and repeated in this experiment, and observed in frozen irradiated ferrioxalate samples. [14] Also in agreement with the ferrioxalate data, additional vibrational energy bands are seen at lower energies (2316 cm^{-1} and 2293 cm^{-1}), can be attributed to vibrationally excited states of CO_2. [17] These hot CO_2 molecules transition to the vibrational ground state within ~40 ps. Photoexcitation of a control iron-free citrate solution in H_2O generated a broad and featureless enhanced-absorption band centered around 2100 cm^{-1} that decayed within 20 ps.

Photoexcitation of Fe-citrate in D_2O caused a prompt and irreversible loss of spectral intensity in the region from 1660–1610 cm^{-1} that overlaps a broader absorbance feature observed in ground-state FTIR data (**Figure 2B**). This region includes vibrational bands associated with asymmetric stretches of carboxylate groups complexed to Fe(III). [14] The different electron-withdrawing strengths of *alpha* versus *beta* hydroxy groups in citrate likely contribute to the width of the FTIR absorbance in this region. The transient signal at 3 ns can be fitted by a single Gaussian peak centered at 1611 cm^{-1} with a width of ~70 cm^{-1}. The loss in optical density at this frequency is thus consistent with loss via decarboxylation. The early transient spectra include an additional negative-going band, centered at 1646 cm^{-1} with a width ~40 cm^{-1}, that decays within ~10 ps (**Figure 2C**). This feature may represent the photoexcitation of carboxylic acid moieties without charge transfer to iron.

We searched for infrared signatures of additional products of photooxidation. Ferrioxalate photolysis generates both CO_2 and the CO_2 radical anion, which was previously detected from an absorption band at approximately 1660-1670 cm^{-1}. [23,24] Fe-citrate photolysis generates CO_2 and is expected to produce the larger organic radical, $C_5H_7O_5^+$, but it was not possible to obtain an infrared signature of this product within the available user facility time. Abrahamson et al described IR spectral changes observed in the UV irradiation of freeze-dried Fe-citrate. [14] Shifts in the vibrational frequencies of the asymmetric and symmetric carboxylic stretch are associated with the altered bonding to iron(II) and not to a new functional group. They report the appearance of a new band at 1710 cm^{-1}, attributed to a ketone group. In this study, however, no vibrational bands within 1800–1550 cm^{-1} are either gained or lost within the timeframe of 3 ns. Further work that

expands both the spectral and temporal ranges will be required to identify and characterize the organic radical product(s) of Fe-citrate photolysis.

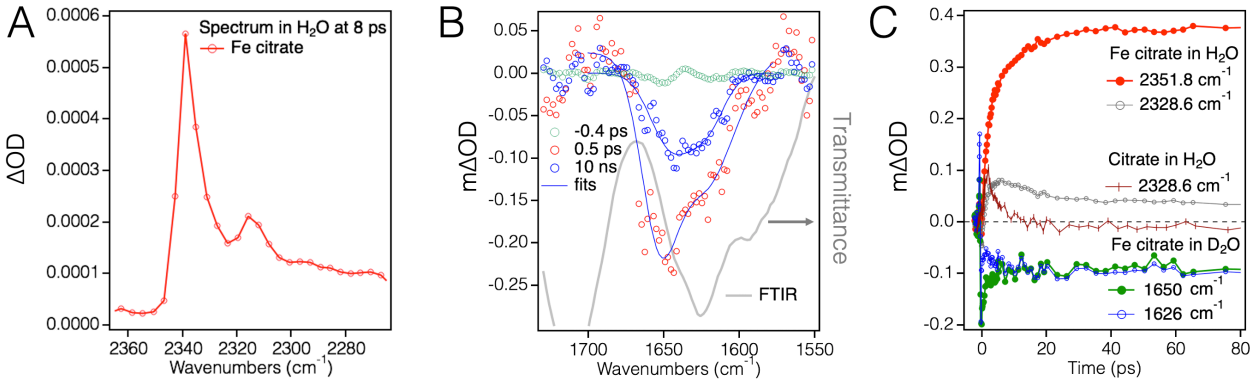

Figure 2 Time-resolved infrared observation of Fe citrate photooxidation. A) Difference vibrational spectrum of Fe citrate in H_2O at 8 ps following photoexcitation. The major peak at 2339 cm^{-1} is at the location of the asymmetric stretch of CO_2 in the vibrational ground state. The shoulders at 2316 cm^{-1} and 2293 cm^{-1} are interpreted as the asymmetric stretch for CO_2 in vibrational excited states. [17] B) Difference vibrational spectrum in D_2O at three time points with 2-Gaussian fits to data at 0.5 ps and 10 ns. Also plotted is the ground-state FTIR spectrum of 20 mM Fe-citrate. C) Kinetic traces tracking the rate of ground-state CO_2 production (monitored at 2363 cm^{-1}), the loss of the vibrationally excited state of CO_2 (monitored at 2328.6 cm^{-1}) and decarboxylation (monitored at 1626 cm^{-1} with an additional, reversible transient loss evident at 1650 cm^{-1}). Also shown is a control trace for iron-free citrate in H_2O.

Photoexcitation of Fe salicylate also generated CO_2. Comparison of the time-resolved infrared data for the three complexes shows identical products (**Figure 3A**) and highly similar dynamics (**Figure 3B**). The intensity of the CO_2 signal, however, varies in the order Fe-salicylate < Fe-citrate < ferrioxalate. In this study, it was not possible to calibrate the IR signal intensity to measure the amount of CO_2 produced per excitation. Nevertheless, because each sample contained the same concentration of iron, and because the photoexcitation fluence was maintained at an approximately constant value, the data show that the quantum yield for prompt CO_2 production is different between samples. The trend in CO_2 yields qualitatively follows the same trend in quantum yields (Φ) for these complexes as measured by the generation of Fe(II).[10,21] For example, at an excitation wavelength of 365 nm, for Fe salicylate, $\Phi = 0.02$; [25] for Fe-citrate, $\Phi = 0.25$; [1] and for Fe-oxalate, $\Phi = 1.25$. [26] Although a different excitation wavelength used in the present study (266 nm), a similar ranking is expected.

It has been proposed that quantum yield of Fe-citrate photolysis, and the variation in CO_2 yields more generally, can be explained by a 3-step kinetic reaction scheme. [25] In this model, a transient photoexcited Fe-carboxylato complex either decays back to the ground state or lyses to produce Fe(II) and an organic radical that promptly decomposes to produce CO_2. In this model, the change in the CO_2 signal would be described by a first-order kinetic rate law.

However, prior studies demonstrated[17,18], using TR-IR and *ab initio* modeling, that photoexcited Fe-oxalate complexes decompose within 1 ps and the change in the CO_2 signal is associated with vibrational cooling of a hot molecular photoproduct. When scaled to account for the different CO_2 signal strengths, kinetics traces for all three complexes overlap up to 1 ns, suggesting similar photoexcitation dynamics in each case (**Figure 3C**). The rates of CO_2 generation were further quantified by fits to the first 60 ps of each time-dependent trace. A bi-exponential model gave better agreement with the data than a first-order kinetic model (**Table 1**), supporting a common model of prompt CO_2 generation and vibrational cooling.

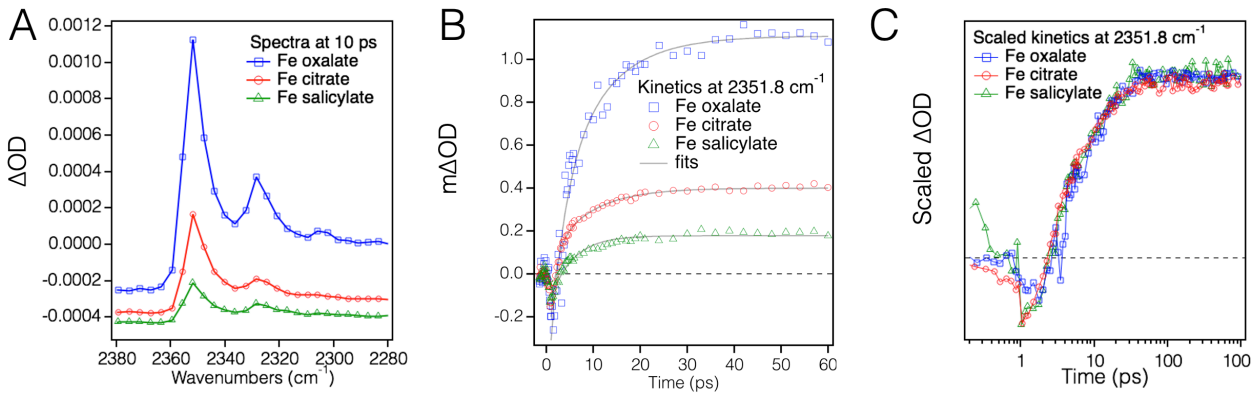

Figure 3 Comparison of the photooxidation of ferrioxalate, Fe salicylate and Fe citrate. A) Difference vibrational spectrum of the three complexes in H_2O at 10 ps following photoexcitation showing a new spectral feature associated with the production of CO_2. B) Time-dependence of the CO_2 signals for the 3 compunds monitored at 2351.8 cm^{-1} with fits of the bi-exponential model described in the text C) Time-dependence of the CO_2 signals for the 3 compounds scaled and plotted on a logarithmic time axis up to 1 ns. Data were shifted by 1 ps for plotting on the log axis.

	Bi-exponential			First order	
Compound	χ^2	k_{10} (ps^{-1})	k_{20} (ps^{-1})	χ^2	k_{1st} (ps^{-1})
Fe oxalate	1.1	1.2 ± 0.2	8.4 ± 0.3	1.5	0.2 ± 0.05
Fe citrate	1.5	2.1 ± 0.3	8.4 ± 0.3	2.2	0.3 ± 0.06
Fe salicylate	0.6	2.3 ± 0.3	10.7 ± 0.9	1.2	0.2 ± 0.06

TABLE 1: Comparison of the χ^2 goodness-of-fit values and rate constants fitted to the time-resolved traces of **Figure 3B** using the bi-exponential model (eqn. 2) or the first order kinetics model (eqn. 1).

CONCLUSIONS

Our results demonstrate a common photo-decarboxylation mechanism for Fe-carboxylate complexes across a range of molecular weights and structures. Specifically, we find that decarboxylation is initiated within a picosecond following photoexcitation, that photoexcitation creates populations of ground-state and hot CO_2 molecules, and that the generation and cooling of CO_2 proceeds to completion within 40 ps. The identical rates are surprising given the different molecular structures of these three ligands. For example, the aromatic ring of salicylate might be expected to stabilize the organic radical in the second step of photo-decarboxylation, delaying CO_2 generation. In fact, however, no such difference is evident in the acquired data. This finding thus suggests that diverse natural hydroxy carboxylate molecules bound to Fe may also have similar kinetics of photo-decarboxylation.

Differences in the CO_2 yield within 50 ps are qualitatively similar to the long-time-scale quantum yield for Fe(II) production, indicating the importance of this initial step for the overall reaction. The present data suggest that a fraction of Fe-citrate photoexcitation events do not lead to ligand-to-metal charge transfer, and better understanding the competition between these different processes may enable decarboxylation yields to be predicted. Of course, overall photo-decarboxylation kinetics observed for different types of natural organic matter[15] are influenced by the subsequent aqueous chemical reactions of the organic radical molecule(s) that are generated by decarboxylation. Time-resolved infrared studies capable of studying such processes beyond the 3-ns window used here are anticipated to greatly inform our understanding of such processes.

Future work may also include testing other environmentally relevant reducible metals capable of ligation by carboxylate moieties, such as copper. [27]

ACKNOWLEDGEMENTS

C.J.W. was supported by an NSF Postdoctoral Fellowship from the Division of Earth Sciences under Award # 1854875. B.G. was supported by the Chemical Sciences, Geosciences, and Biosciences Division, of the U.S. Department of Energy (DOE) under Contract No. DE-AC02-05CH11231. R.D.S. and use of the Center for Nanoscale Materials, an Office of Science user facility, were supported by the U. S. Department of Energy, Office of Science, Office of Basic Energy Sciences, under Contract No. DE-AC02-06CH11357.

REFERENCES

(1) Faust, B. C.; Zepp, R. G. Photochemistry of Aqueous Iron(III) Polycarboxylate Complexes - Roles in the Chemistry of Atmospheric and Surface Waters. *Environmental Science & Technology* **1993,** 27, 2517-2522.

(2) Pang, H. *et al.* Photochemical Aging of Guaiacol by Fe(III)–oxalate Complexes in Atmospheric Aqueous Phase. *Environmental Science & Technology* **2018**, 53, 127-136.

(3) Mopper, K. *et al.* Photochemical Degradation of Dissolved Organic Carbon and its Impact on the Oceanic Carbon Cycle. *Nature* **1991**, 353, 60-62.

(4) Cory, R. M.; Ward, C. P.; Crump, B. C.; Kling, G. W. Sunlight Controls Water Column Processing of Carbon in Arctic Fresh Waters. *Science* **2014**, 345, 925-928.

(5) West, C. P. *et al.* Molecular investigation of the Multi-phase Photochemistry of Fe(III)–citrate in Aqueous Solution. *Environmental Science: Processes & Impacts* (2023).

(6) Waite, T. D.; Morel, F. M. Ligand Exchange and Fluorescence Quenching Studies of the Fulvic Acid-Iron Interaction: Effects of pH and Light. *Analytica Chimica Acta* **1984**, 162, 263-274.

(7) Bertilsson, S.; Tranvik, L. J. Photochemical Transformation of Dissolved Organic Matter in Lakes. *Limnology and Oceanography* **2000**, 45, 753-762.

(8) Garg, S.; Jiang, C.; Waite, T. D. Mechanistic Insights into Iron Redox Transformations in the Presence of Natural Organic Matter: Impact of pH and Light. *Geochimica et Cosmochimica Acta* **2015**, 165, 14-34.

(9) Porcal, P.; Amirbahman, A.; Kopáček, J.; Novák, F.; Norton, S. A. Photochemical Release of Humic and Fulvic Acid-Bound Metals from Simulated Soil and Streamwater. *Journal of Environmental Monitoring* **2009**, 11, 1064-1071.

(10) Karlsson, T.; Persson, P.; Skyllberg, U.; Mörth, C.-M.; Giesler, R. Characterization of Iron(III) in Organic Soils using Extended X-ray Absorption Fine Structure Spectroscopy. *Environmental Science & Technology* **2008**, 42, 5449-5454.

(11) Daugherty, E. E.; Gilbert, B.; Nico, P. S; Borch, T. Complexation and Redox Buffering of Iron(II) by Dissolved Organic Matter. *Environmental Science & Technology* **2017**, 51, 11096-11104.

(12) Gao, H.; Zepp, R. G. Factors Influencing Photoreactions of Dissolved Organic Matter in a Coastal River of the Southeastern United States. *Environmental Science & Technology* **1998**, 32, 2940-2946.

(13) Weller, C.; Horn, S.; Herrmann, H. Photolysis of Fe(III) Carboxylato Complexes: Fe(II) Quantum Yields and Reaction Mechanisms. *Journal of Photochemistry and Photobiology A: Chemistry* **2013**, 268, 24-36.
(14) Abrahamson, H. B.; Rezvani, A. B.; Brushmiller, J. G. Photochemical and Spectroscopic Studies of Complexes of Iron(III) with Citric Acid and other Carboxylic Acids. *Inorganica Chimica Acta* **1994**, 226, 117-127.
(15) Ward, C. P.; Cory, R. M. Complete and Partial Photo-oxidation of Dissolved Organic Matter Draining Permafrost Soils. *Environmental Science & Technology* **2016**, 50, 3545-3553.
(16) Strobel, B. W. Influence of Vegetation on Low-Molecular-Weight Carboxylic Acids in Soil Solution—a Review. *Geoderma* **2001**, 99, 169-198.
(17) Mangiante, D. M.; Schaller, R. D.; Zarzycki, P.; Banfield, J. F.; Gilbert, B. Mechanism of Ferric Oxalate Photolysis. *ACS Earth and Space Chemistry* **2017**, 1, 270-276.
(18) Straub, S.; Brünker, P.; Lindner, J.; Vöhringer, P. Femtosecond Infrared Spectroscopy Reveals the Primary Events of the Ferrioxalate Actinometer. *Physical Chemistry Chemical Physics* **2018**, 20, 21390-21403.
(19) Pozdnyakov, I. P.; Kel, O. V.; Plyusnin, V. F.; Grivin, V. P.; Bazhin, N. M. New Insight into Photochemistry of Ferrioxalate. *The Journal of Physical Chemistry A* **2008**, 112, 8316-8322.
(20) Chen, J. *et al.* Transient Structures and Kinetics of the Ferrioxalate Redox reaction studied by Time-resolved EXAFS, Optical Spectroscopy, and DFT. *The Journal of Physical Chemistry A* **2007**, 111, 9326-9335.
(21) Gautier-Luneau, I. *et al.* New Trends in the Chemistry of Iron(III) Citrate Complexes: Correlations between X-ray Structures and Solution Species probed by Electrospray Mass Spectrometry and Kinetics of Iron Uptake from Citrate by Iron Chelators. *Chemistry–A European Journal* **2005**, 11, 2207-2219.
(22) Diroll, B. T.; Guo, P.; Chang, R. P.; Schaller, R. D. Large Transient Optical Modulation of Epsilon-near-zero Colloidal Nanocrystals. *ACS Nano* **2016**, 10, 10099-10105.
(23) Jacox, M. E.; Milligan, D. E. Vibrational Spectrum of CO_2^- in an Argon Matrix. *Chemical Physics Letters* **1974**, 28, 163-168.
(24) Zhou, M.; Andrews, L. Infrared Spectra of the CO_2^- and $C_2O_4^-$ Anions Isolated in Solid Argon. *The Journal of Chemical Physics* **1999**, 110, 2414-2422.
(25) Pozdnyakov, I. P. *et al.* Photophysics of Fe(III)–tartrate and Fe(III)–citrate Complexes in Aqueous Solutions. *Chemical Physics Letters* **2012**, 530, 45-48.
(26) Hatchard, C. G.; Parker, C. A. A New Sensitive Chemical Actinometer. 2. Potassium Ferrioxalate as a Standard Chemical Actinometer. *Proceedings of the Royal Society of London Series A-Mathematical and Physical Sciences* **1956**, 235, 518-536.
(27) Agterberg, F.; Driessen, W.; Reedijk, J.; Oeveringb, H.; Buijs, W. Copper-catalyzed Oxidative Decarboxylation of Aliphatic Carboxylic Acids. *Studies in Surface Science and Catalysis* **1994**, 82, 639-646.

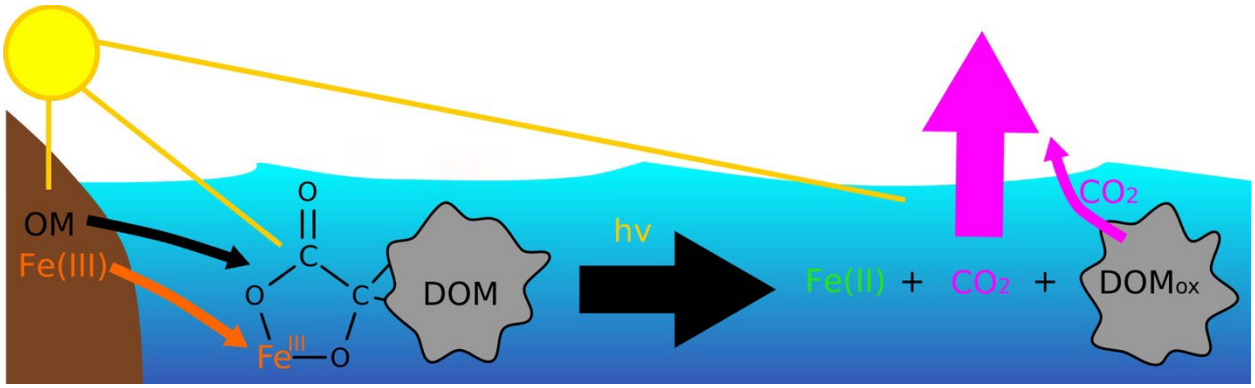

TOC Graphic